2-9-2010

Planar and oblique shock wave interaction with a droplet seeded gas cylinder

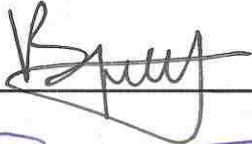Evan Johnson

Evan P.R. Johnson
Candidate

Mechanical Engineering
Department

This thesis is approved, and it is acceptable in quality and form for publication:

Approved by the Thesis Committee:

_____ ,Chairperson

C Randall Truman

_____

Planar and oblique shock wave interaction with a droplet seeded gas cylinder

by

Evan PR Johnson

B.S., Mechanical Engineering, University of New Mexico, 2007

THESIS

Submitted in Partial Fulfillment of the

Requirements for the Degree of

Master of Science
Mechanical Engineering

The University of New Mexico

Albuquerque, New Mexico

December, 2009

Acknowledgments

I would like to acknowledge all of those who encouraged me, assisted me, and inspired me during the writing of my Master's thesis. Without the help from God, family, friends, and colleagues none of this would have been possible. A special thanks to Riccardo Bonazza for creating the online $WiSTL$ gas dynamics calculator that assisted in checking calculations for my thesis.

Planar and oblique shock wave interaction with a droplet seeded gas cylinder

by

Evan PR Johnson

ABSTRACT OF THESIS

Submitted in Partial Fulfillment of the
Requirements for the Degree of

Master of Science
Mechanical Engineering

The University of New Mexico

Albuquerque, New Mexico

December, 2009

Planar and oblique shock wave interaction with a droplet seeded gas cylinder

by

Evan PR Johnson

B.S., Mechanical Engineering, University of New Mexico, 2007

M.S., Mechanical Engineering, University of New Mexico, 2009

Abstract

We present an experimental study of a shock interaction with an initially diffuse heavy-gas cylinder seeded with submicron-scale glycol droplets. Unlike most earlier studies, the investigation covers not just a quasi-two-dimensional geometry, where the axis of the cylinder is parallel to the plane of the shock, but also the oblique interaction at an angle of 15° between the cylinder axis and the plane of the shock wave. Our experimental data cover the range of Mach numbers from 1.2 to 2.4. The heavy gas cylinder is produced by injecting sulfur hexafluoride pre-mixed with glycol vapor into the test section of a tiltable shock tube through a co-flowing nozzle, with the gravity-driven flow of the heavy gas stabilized by an annular flow of air in the downward direction. Droplets in the gas cylinder are visualized via Mie scattering of diffuse white light. Two views of the flow – side and top – are simultaneously

captured by a high-speed gated and intensified CCD camera, producing a spatially and temporally resolved description of the evolution of the gas cylinder upon impulsive acceleration. While the observations for the planar interaction reveal that the large-scale flow structure remains largely two-dimensional, confirming the assumptions of earlier studies, during the oblique shock interaction, we observe evidence of flow evolution in three dimensions, including asymmetric interaction of the gas cylinder with the boundary layers forming on the walls of the shock tube, and rotation of this cylinder in the vertical plane parallel to the streamwise direction.

Contents

Contents

List of Figures

Glossary

ρ_1 Density before the shock wave

ρ_2 Density after the shock wave

γ Heat capacity ratio

M_1 Mach number before the shock wave

M_2 Mach number after the shock wave

p_1 Pressure before the shock wave

p_2 Pressure after the shock wave

v_1 Specific volume before the shock wave

v_2 Specific volume after the shock wave

T_1 Temperature before the shock wave

T_2 Temperature after the shock wave

Chapter 1

Introduction

Richtmyer-Meshkov Instability (RMI) occurs when an interface between fluids of contrasting densities is impulsively accelerated. One method of impulsive acceleration is the passage of a shock wave through the fluid interface. The development of the instability begins with perturbations that are small in amplitude which initially grow linearly with time. This is followed by a nonlinear regime with "bubbles" appearing on the side of a light fluid penetrating a heavy fluid, and with "spikes" appearing on the side of a heavy fluid penetrating a light fluid. A turbulent regime eventually is reached and the two fluids mix. In our experiments we see the RMI, but with some added complexities due to the presence of liquid droplets. Modeling a compressible multiphase flow with mixing gases and particle/droplet phases is relevant to our work in addition to other applications. Some of these applications include modeling conditions inside of internal combustion engines, rocket engines, and inertial confinement fusion. Our work will benchmark different phenomena that occur when a shock wave accelerates a gas cylinder that is at an oblique angle to the shock front itself. Our initial conditions are three-dimensional, not nominally two-dimensional like most earlier experiments that have been done.

Multiple complex physical phenomena have to be taken into consideration which occur when an oblique shock wave interacts with a density interface. Several insta-

bilities are introduced which interfere with one another, adding more complexity to the interaction. If a constant normal acceleration is present it feeds energy to the Rayleigh-Taylor (RT) instability or, depending on the sign of gA (g=acceleration, A=Atwood number), it acts to stabilize the KH and RM instabilities [1]. In this thesis, I will present our experimental/diagnostic set up, results of our experiments, as well as observations and future planned experiments.

1.1   Governing Equations

The following equations describe the conditions before and after the shock wave. We can use them to determine certain quantities and compare them to our experimental results. From one side of the shock wave to the other, there are significant differences in pressure, density, and temperature among other properties.

The following equations are fundamental to our study of shock waves and particle interactions. They describe the conditions before (subscript 1) and after (subscript 2) the shock. In this section, the nomenclature and equations follow Landau and Lifshitz [2]. The density change is direct result of gas compression [2]:

$$\frac{\rho_2}{\rho_1} = \frac{(\gamma + 1) M_1^2}{(\gamma - 1) M_1^2 + 2} \tag{1.1}$$

The pressure jump in the gas leads to compression of the particulate phase [3]:

$$\frac{p_2}{p_1} = \frac{2\gamma}{\gamma + 1} M_1^2 - \frac{\gamma - 1}{\gamma + 1} \tag{1.2}$$

The temperature jump in gas leads to the heating of the specimen under test, *e.g.*. particles, droplets, etc. [2]:

$$\frac{T_2}{T_1} = \frac{\left[2\gamma M_1^2 - (\gamma - 1)\right]\left[(\gamma - 1) M_1^2 + 2\right]}{(\gamma + 1)^2 M_1^2} \tag{1.3}$$

The Mach number M_2 is given in terms of M_1 [2] as

$$M_2^2 = \frac{2 + (\gamma - 1)\, M_1^2}{2\gamma M_1^2 - (\gamma - 1)} \tag{1.4}$$

We can give limiting results for very strong shock waves, in which $(\gamma - 1)\, p_2$ is very large compared with $(\gamma + 1)\, p_1$ [2]:

$$\frac{\rho_1}{\rho_2} = \frac{\gamma - 1}{\gamma + 1} \tag{1.5}$$

$$\frac{T_2}{T_1} = \frac{(\gamma - 1)\, p_2}{(\gamma + 1)\, p_1} \tag{1.6}$$

The ratio T_2/T_1 increases to infinity as p_2/p_1 increases [2]. Thus, the temperature discontinuity in a shock wave, like the pressure discontinuity, can be arbitrarily high. The density ratio tends to a constant limit. For a monatomic gas the limit is $\rho_2 = 4\rho_1$ [2].

While these equations are sufficient for single phase gaseous flows, the addition of particles or droplets changes the flow physics, especially during the transition to turbulence. There are many applications where the dispersion of particles in turbulent shear flows is of great interest and importance. The injection of gasoline in an internal combustion engine, for example, is a very important application. Some others include particle spray in rocket engines, flow of concrete in transportation pipes, and pollutants in the air or bodies of water. Depending on the mass loading of particles that exist in a particular flow, they can actually modify the turbulence structure in the carrier fluid [4]. In our shock tube experiments, the injection of a Sulfur Hexafluoride (SF_6) gas cylinder seeded with glycol droplets qualifies as a particle laden flow. Understanding the influence of the particles on the turbulence structures could prove extremely useful in characterizing certain observed flow phenomena.

Elghobashi [4] realized that the prediction of these transport phenomena requires knowledge of the two-way nonlinear coupling between the particles and turbulence,

i.e. the response of the discrete particles to the turbulent motion of the fluid, and the effect of the particles motion on the frequency spectrum of turbulence [4]. Elghobashi used a direct numerical simulation (DNS) to predict turbulent flows laden with solid particles. He defined several quantities that characterize the effects that the particles will have on the flow. Depending on the particle size, concentration, and spacing between one another, the particles have different effects on the flow. "One-way-coupling", "two-way-coupling", or "four-way-coupling" are terms that were used to designate the interaction between the particles and turbulence. In one-way-coupling, the particle dispersion depends on the state of turbulence but there is no feedback to the turbulence itself. Two-way-coupling is second regime where the particle loading is large enough to alter the turbulence structure. In this regime there is an increased dissipation rate of turbulence energy as the diameter of the particle decreases for the same particle material and fluid viscosity. However, as the particle response time increases for a given particle volume fraction, the particle Reynolds number increases and vortex shedding takes place resulting in enhanced production of turbulence energy [4].

Flows that fall into one and two-way coupling are often referred to as dilute suspensions. In four-way-coupling, the particle loading is large enough that there are actually particle/particle collisions that take place, hence the term four-way-coupling. Due to the particle loading in these flows, they are often referred to as dense suspensions. The flows are very complex in this regime, so most studies are conducted using dilute suspensions [4].

DNS provides a modeling-free, three-dimensional, instantaneous velocity field for the fluid in simple turbulent flows. This velocity field can be used to calculate the three-dimensional trajectory of a particle from which the dispersion statistics can be obtained [4]. This work showed that depending on the particle characteristics, mass loading in the flow, and the carrier fluid, particles can actually alter the turbulence structure in a shear flow. However, at the present state of the art, while DNS can be used to understand local particle dynamics, spatially resolved DNS of a multiphase

mixing flow on large scales remains prohibitively computationally expensive, thus requiring different models (such as large eddy simulation, or LES), which have closure assumptions necessitating benchmarking with experimental results.

The following section focuses on the Richtmyer-Meshkov instability when the particulate phase is either not considered, not present, or is present as a tracer (in one-way coupling regime). Experiments related to turbulent mixing and baroclinic vorticity generation are also discussed. Since all of the aforementioned topics relate to our shock tube experiments, a good understanding of these topics will help us to interpret the results and observations of our experiments.

1.2 Shock-driven evolution of gaseous interfaces: earlier work

As discussed earlier, the RMI arises when a density gradient in a fluid (gas) is subjected to an impulsive acceleration (e.g., due to a shock wave passage). The evolution of RMI is non-linear and hydrodynamically complex and hence is a very good test problem to validate numerical codes. In a paper by Palekar et al. [5], a two-dimensional numerical simulation of RMI-driven evolution of the flow produced by shock acceleration of a diffuse heavy gaseous cylinder embedded in lighter gas is presented. Comparison of the late-time flow statistics between experiment and numerics elucidated the limitations inherently present in a two-dimensional simulation of a spatially three-dimensional flow, even if the large-scale flow structure is nominally two-dimensional [5].

This section focuses on the Richtmyer-Meshkov instability when the particulate phase is either not considered, not present, or is present as a tracer (in one-way coupling regime). This interfacial instability was theoretically predicted by a Los Alamos theorist Richtmyer (1960) [6], and first experimentally observed by a Russian exper-
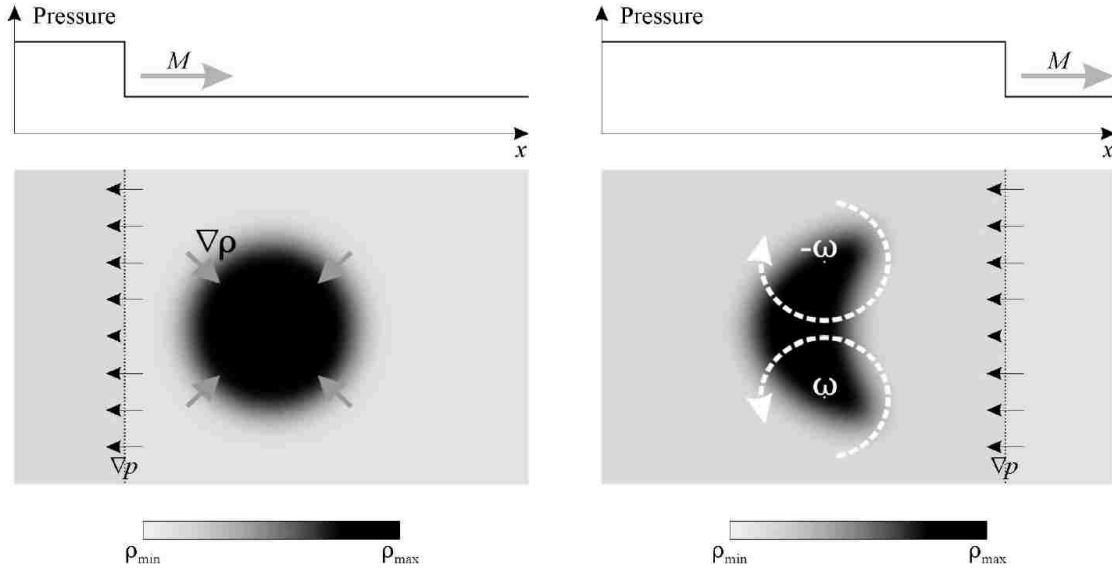
Figure 1.1: Simplified representation of a planar shock acceleration of an initially diffuse cylindrical density interface: left - before the acceleration, right - after the acceleration. The initial misalignment between gradients of pressure (black arrows) and density (grey arrows) leads to deposition of vorticity (white dashed arrows). After Palekar et al. [5].

imentalist working in VNIIEF (Sarov), Meshkov (1969) [7]. The fluid configuration leading to a frequently considered RMI problem is shown in Fig. 1.1. Two fluids with different properties are separated by an initially diffuse interface. The shock travels from light fluid (gray color) to heavy fluid (black color) through the interface.

Summarizing previous studies, Palekar et al. [5] described the development of RMI in this configuration as following a three-stage process of evolution. the short initial stage is linear. In this stage, the incident shock wave collides with a perturbed material interface and bifurcates into a transmitted shock and a reflected wave. In Fig. 1.1, left, the pressure and density gradients are locally misaligned. This misalignment leads to baroclinic generation of vorticity at the interface. The resulting vortex roll-up (Fig. 1.1, right) leads to growth of the perturbation amplitude of the interface. The flow-field in this stage is deterministic. Later in this stage, spikes and bubbles appear on the interface. A bubble is a portion of the light fluid penetrating

into the heavy fluid and a spike is a portion of the heavy fluid penetrating into the light fluid. The second stage is non-linear deterministic. In this stage the spikes and bubbles grow substantially. The amplitude of perturbation grows to the order of the wavelength and hence now the flow is non-linear. In the later part of this stage, roll-up of material into the vortex cores occurs. Roughly at the same time, small scales also appear in the flow. In the third stage, the secondary instabilities become pronounced and lead to the onset of turbulence with chaotic mixing. Being turbulent in nature, this stage is dominated by three-dimensional physics, unlike the first two stages [5].

The classical Rayleigh-Taylor and Kelvin-Helmholtz instabilities refer to the exponential growth of interface perturbations under the action of a constant acceleration and under the action of shear, respectively. A shock normal to the interface induces an impulsive acceleration and triggers the Richtmyer-Meshkov instability which grows linearly in time, provided there is no post-shock acceleration or shear. Mikaelian [1] derived analytical expressions using a generalization of Richtmyer's technique. This meant treating the shock as an instantaneous acceleration of incompressible fluids. This was mainly to avoid the complexity of the fully compressible problem. As mentioned earlier, the problem of an oblique shock on a plane interface is well known, and the problem of a normal shock on a perturbed interface (the Richtmyer-Meshkov problem) is also quite familiar, the combined problem of an oblique shock on a perturbed interface remains unsolved [1].

Mikaelian considered two fluids having different densities and horizontal directed velocities, resulting from the induced perturbation. The fluid interface lies in the $x - z$ plane. Through several complex mathematical expressions involving densities, velocities, wave numbers, and an expression for the perturbation as a function of time, Mikaelian was able to describe the evolution of the perturbation at an interface after an oblique shock strike changed the normal velocity and parallel velocities. Both instantaneous as well as subsequent steady evolution expressions were derived. Some applications for this work were in inertial-confinement-fusion (ICF) capsules.

Due to the amplification of the perturbation upon re-shock (when the shock is reflected back through the interface) it was proposed that this amplification was a possible mechanism for mixing in ICF capsules. In a typical ICF capsule, the fuel is a solid DT (Deuterium-Tritium) shell surrounding a very low-density sphere of gaseous DT, the spark plug. At this interface the density contrast is usually very large, thus making the RM instability dominant [1]. Mikaelian noticed that unless the first shock is immediately followed by acceleration the KH term, which is always positive, would dominate. He concluded that the interplay between RT, KH, and RM instabilities is complicated by the fact that they all have different dependence on different wave numbers (relating to the induced interface perturbations) and the compressible situation is obviously much more complex, even in the completely linear regime.

Yang et al. [8] studied the results of direct numerical simulations of inviscid planar shock-accelerated density stratified interfaces in two dimensions and compared them to previously conducted shock tube experiments. Heavy-to-light (slow/fast or s/f) and light-to-heavy (fast/slow, or f/s) gas interfaces were examined and early-time impulsive vorticity deposition and the evolution of coherent vortex structures were emphasized and quantified [8]. They determined that a second-order numerical Godunov scheme yielded excellent agreement with shock-polar analysis at early time. A more physical vortex interpretation explains the commonly used (i.e. linear paradigm) designations of unstable and stable for the f/s and s/f interfaces, respectively. In this work, there are some correlations to the work by Mikaelian in that they both are interested in RT instabilities. However Yang et al. were more interested in describing the RT instability in terms of a vortex layer (large-scale translation and rotation), asymmetric tip vortex roll-up and binding, layer instability, convective mixing, and baroclinic vorticity generation from secondary shock-interface interactions [8].

Yang et al. were particularly interested in the early-time stability and the longer-term evolution of a shock-accelerated interface. Yang et al. considered two cases.

Both were characterized by a shock wave propagating through a fluid of one density, striking a contact interface, and passing into a region of a different density, where the two regions are initially in pressure balance. They defined the setup in terms of sound speed or wave impedance for a physically meaningful reason. The results of a linear stability analysis showed that the s/f interaction is stable and the f/s interaction is unstable. Whether an interaction is considered stable or unstable is relative to the length of the term being considered, which if it is too large, the surfaces of both interactions become increasingly distorted (unstable).

Many analytical efforts have been confined to early time event or small infinitesimal perturbations so that advantage can be taken of linearity. However, beyond the early time events and small infinitesimal perturbations, both s/f and f/s interfaces depart drastically from their initial configurations. When an interface is deemed either stable or unstable, this can be misleading since it is only deemed such for a very short period of time. Collision of two vortex layers of opposite signs was used to model this. Yang et al. focused mainly on the primary and secondary features for the shock-single-interface interaction as well as demonstrating that the initial deposition of vorticity can be describe quantitatively by a shock-polar analysis (SPA), when the latter provides solutions [8].

Yang et al. [8] used the conservative form of Euler equations in two dimensions, namely the mass, momentum, and energy conservation equations for an inviscid, compressible fluid to model the shock tube experiments. Initially they separated the two gases of different densities by a sharp interface. In experiment, this would correspond to a membrane or some similar gas separation method. By contrast, in our experiments described in the following chapters, the density interface is gravity-stabilized and initially diffuse. The interface is oriented so that it lies at a 15° angle from the vertical (Fig. 1.2).

While Fig. 1.2 refers to $M = 1.2$, studies have also been performed with increased Mach number and incident shock angle. As either the Mach number or incident shock
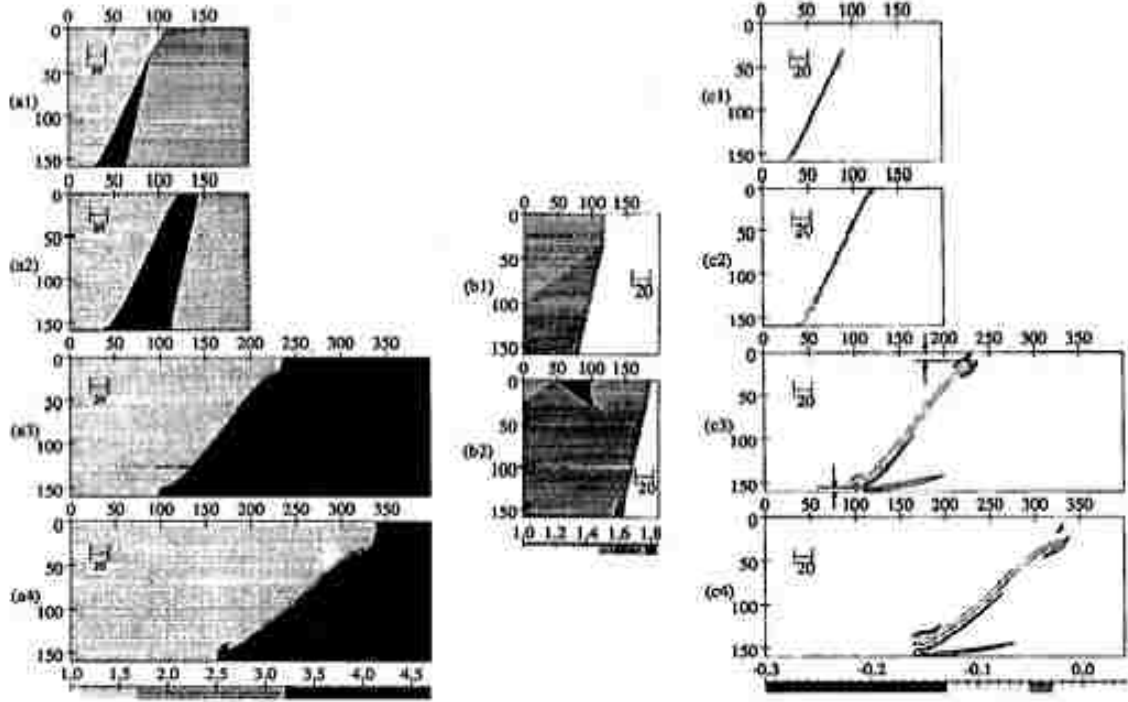
Figure 1.2: Images for a M=1.2 shock interacting with an f/s interface where the density ratio is equal to 3 and interface-shock plane angle *theta* is equal to 30°, after Yang et al. [8]. Presented is a time sequence: density (a1)-(a4) left column; pressure (b1) and (b2), center column; and vorticity (c1)-(c4), right column. The times for these images are row 1, $t = 13.83$ (100); row 2, $t = 27.50$ (200); row 3, $t = 109.05$ (800), and row 4, $t = 192.15$ (1400). Direction of the flow is from left to right. From Yang et al. [8].

angle are increased for a f/s interaction, the processes are stronger and more rapid. To simulate the flow field, Yang et al. used a second-order Godunov scheme which is very suitable for problems involving complicated nonlinear wave interactions [8]. At a later time once the shock has propagated, the interface rotates away from the wall of the tube and it is evident that there is breaking of symmetry, since the location of the upper layer tip is farther from the wall than the lower tip. The difference is mainly due to the interaction of the interface with the following two positive weak vortex sheets of different strengths: one is at the lower boundary; the other is at the upper boundary. These are caused by bent transmitted and bent shock waves respectively. Additionally, these shocks also emit a reflected shock

interacting with the interface. The changes in pressure due to these phenomena are relatively weak. The interface is essentially a shear layer, and if it is sufficiently strong, vortical rollers will develop as a result of the nonlinear growth of the KH instability. Note that interface stretching is a stabilizing phenomenon postponing the appearance of rollers [8]. Several different configurations were used including various fluids such as air, helium, and $R22$ refrigerant (Freon) in different configurations to obtain either a f/s or s/f interface. Yang et al. demonstrated the importance of shock-polar analysis and a vorticity interpretation of physical trends. They found a good agreement between their numerical simulations and experimental investigations.

Further studies by Samtaney and Zabusky [9] were conducted on the shock polar analysis and analytical expressions for vorticity deposition in shock-accelerated density-stratified interfaces. Vorticity is deposited due to baroclinic effects on the surface of a density-stratified interface accelerated by a shock. An analytical expression was presented, derived from shock polar analysis, for circulation per unit length on a fast-slow planar density interface inclined at an angle to the incident shock [9]. Samtaney and Zabusky used an integration of their analytical expression to yield total circulation on non-planar interfaces (sinusoidal and semicircular interfaces) accelerated by shocks. Their results correlated strongly with the diagnostics they obtained from numerical experiments using a second-order Godunov code for the Euler equations.

Elemental processes that occur between a shock wave and a density inhomogeneity are of practical interest in combustion and inertial confinement (laser driven) fusion. Of special interest is the early-time stability and growth rate for shock-accelerated interfaces, which may be explained from the point of view of vortex dynamics [9]. Samtaney and Zabusky believed that accurate quantification of vorticity generation is a very important goal. In this particular experiment they presented analytical expressions for circulation at fast-slow planar gas interfaces using shock polar analysis. With those results they predicted analytically the circulation on non-planar interfaces (sinusoidally perturbed interfaces and bubbles), see Fig. 1.2. They

found a strong agreement between their analytical results and their numerical experiments. Samtaney and Zabusky used problem settings similar to those of Yang et al. A rectangular shock tube with a shock wave propagating through it into a gas of density 1 and an interface separating a gas of density 2 was modeled. Three different possible physical situations were a planar interface inclined at an angle α; a sinusoidally perturbed vertical interface with amplitude A and wavelength λ; or a bubble of radius r_0. Effects of viscosity and changes in specific heat ratio were omitted, as they played a minor role in this parameter domain. As in the simulations by Yang et al., there were two generic classes of interactions that exist. One in which the shock crosses into a fluid with a higher sound speed (i.e. lower density, referred to as the slow/fast or s/f interaction) and the case where the shock passes into a region with a lower sound speed (i.e. higher density, referred to as the fast/slow or f/s interaction). They, however, only considered the f/s interaction for this particular set of simulations (Fig. 1.3).

In shock-polar analysis (SPA) one assumes a frame of reference, which is stationary, with respect to the node where all the shocks meet [9]. They assumed also that initially, both gases are perfect, inviscid, and of constant identical specific heat ratio (γ). Through using analytical expressions that are functions of parameters such as incident (where angle of incidence is α), reflected, and transmitted shocks, streamlines, deflections of shocks, pressures, and Mach numbers, they then derived the SPA equation, which was used to obtain the analytical results. After showing the normalized circulation per unit of length of the interface and the numerical result for a density ratio of 3, Mach number of 1.05 and 2.0, it was apparent that the SPA result terminates at a certain critical angle while the approximate result can be extended to $\alpha = \pi/2$, see Fig. 1.4 [9]. At a large α, the agreement was better for moderate to large Mach numbers. Similar observations were made for large density ratios (Fig. 1.5). A significant source of error arises from comparing the SPA vortex sheet results with an evolving vortex that spreads because of numerical diffusion [9]. This means that for a larger α, the error is expected to be larger as well.
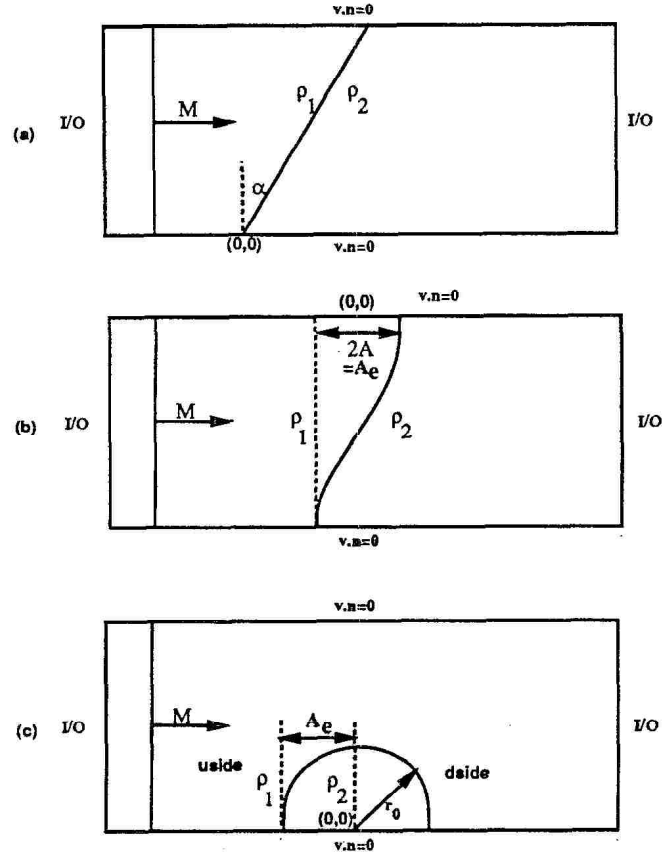
Figure 1.3: Schematic of physical domain and parameters in shock accelerated density stratified interfaces. (a) Planar interface; (b) sinusoidally perturbed interface; and (c) circular interface. From Samtaney and Zabusky [9].

From this work, exact and approximate analytical expressions for circulation deposited on a fast-slow interface accelerated by a shock were presented. Analytical expressions were obtained for vorticity deposition on sinusoidally perturbed and circular interfaces that are in good agreement with numerical results [9]. Samtaney and Zabusky intended to continue work and show where changes in the ratio of the specific heats of the two gases across the interface do not significantly effect the circulation of vorticity. Additionally, they used analytical expressions to develop models to predict the vorticity deposition in shock-bubble interactions and for slow-fast interfaces. For sinusoidally perturbed interfaces, they used the expression for circulation and related it to the growth rate of perturbations in the RMI environment [9].
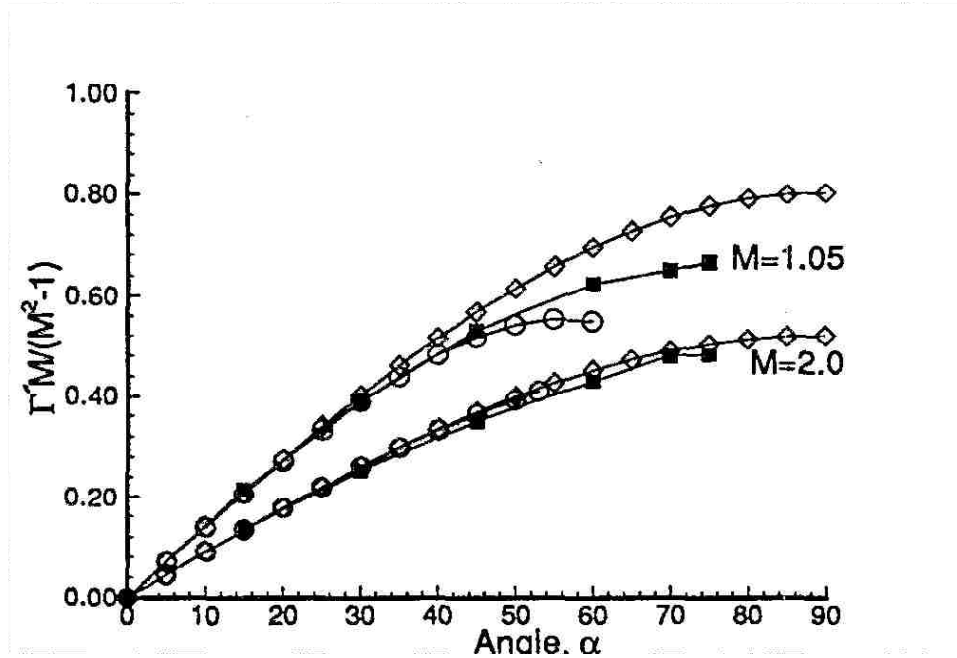
Figure 1.4: Circulation per unit original length for M=1.05 and M=2.0. The circles, diamonds, and squares represent the exact circulation, approximate circulation, and filled numerical circulation, respectively, Samtaney and Zabusky [9].

Studies have been performed on the effects of droplets interacting with oblique shock waves. The main point of one study in particular was to show the breaking-up effects of droplets when they passed through a straight oblique shock wave. In a study by Utheza et al. [10], it was expected that by the addition of particles that the initial slope of the shock wave would change and in some cases that the shock would turn into a compression zone. They noted that among many numerical gas-particles flow simulations proposed in literature, the "two fluids model" had often been retained. This model said that both the gaseous and dispersed phases are each considered to be a distinct continuous medium. Through the particle surface, momentum and energy were exchanged through viscosity and the thermal conductivity [10]. Other researchers gave distinct mechanisms for the fragmentation of a liquid droplet in gas flow [11].

In the study by Utheza et al. [10], it was assumed that the flow was unsteady and

14
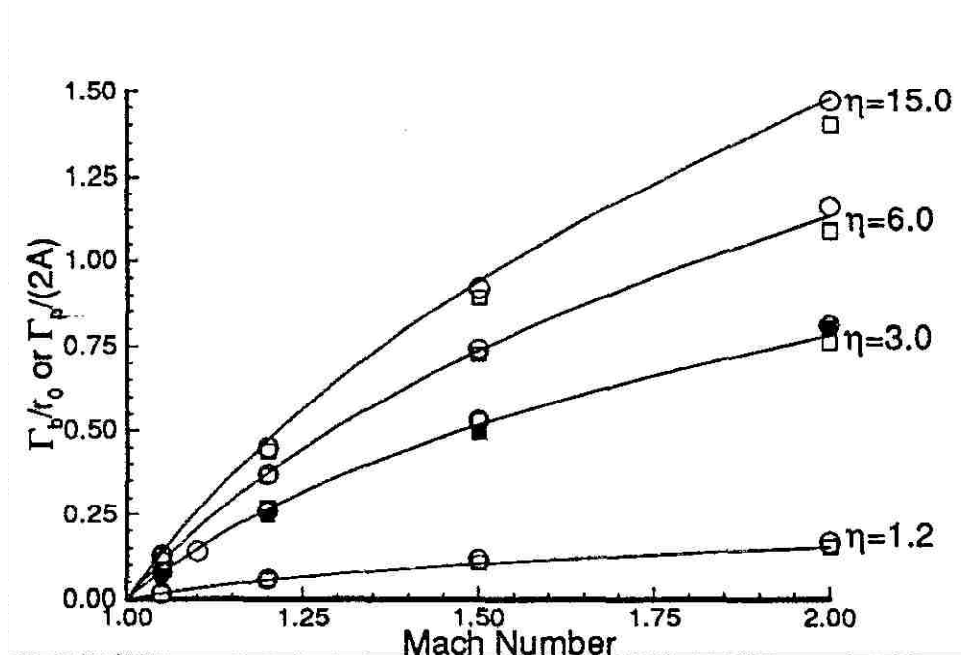
Figure 1.5: Circulation for sinusoidal interface and the "U-side" of the circular bubble for density ratios of 1.2, 3.0, 6.0, and 15.0. Open squares indicate the sinusoidal interface with amplitude of 10 and wavelength of 80. Filled squares indicate the sinusoidal interface with amplitude of 40 and wavelength of 80. Circles indicate the circular bubble. Solid line represents the analytical result. From Samtaney and Zabusky [9].

two-dimensional, the compressible phase was exclusively constituted of steam and followed the ideal gas law, real fluid effects were taken into account only at liquid vapor interfaces, droplets were spherical and incompressible, at a given space point droplets had the same size, speed, and temperature, droplet-droplet interactions were not considered, and the volume occupied by droplets was small. The influence of a two-phase oncoming flow around a wedge where an attached stationary shock wave has developed was studied. The authors of this study investigated mainly the process of particle break-up and its effects on the oblique and straight initial shock. For $t < 0$, the flow around the wedge was a one-phase flow (water steam only). For each case the initial conditions of the two dimensional one phase flow were such that an attached shock wave exists at the tip of the wedge. At $t = 0$, the dispersed phase (droplets) was introduced upstream of the initial location of the stationary shock wave. The

two-phase flow consisted of steam (gaseous phase) and water droplets (dispersed phase) which were assumed to be spherical, mono-dispersed. Upon modeling the flow mathematically and verifying the results numerically, they were able to simulate a gas-particle flow passing through a straight oblique shock wave. Their analysis allowed them to emphasize a certain number of original and noticeable results. These results included that generally, introducing particles in the flow weakens the shock wave. This was accentuated by droplet break-up occurring across the shock wave. The shock wave was weaker when mass and heat transfers were considered in addition to drag force. Also, the addition of the droplet break-up process accentuated the weakening of the shock wave. Particles became smaller after break-up if only the drag forces were taken into account [10].

This work could prove useful in our later studies and attempts to explain and understand the different phenomena that occur when an oblique shock wave interacts with a droplet-seeded gas cylinder. Since our gas cylinder is seeded with small glycol droplets which can be assumed to be spherical, close correlations can be made to give reason as to why certain phenomena are occurring. For example, in the oblique experiments section of Chapter 3 of this thesis, it is mentioned that some of the droplet-seeded gas cylinder material is advected into the boundary layer of the test section in our shock tube. Reasons for this could be very closely related to those verified by Utheza et al. Moreover, a slight bow develops in the gas cylinder as well, possibly due to drag forces or boundary layer interaction with the gas cylinder itself.

Krivets et al. [12] used a vertical shock tube to study the single-mode three-dimensional RMI. The interface was formed using opposed flows of air and SF_6 and the perturbation was created by the periodic motion of the gases within the shock tube. They used Planar laser induced fluorescence for flow visualization. Then they compared their experimental results which were obtained with a shock Mach number of 1.2 with a three-dimensional numerical simulation [12].

A code called Raptor, a multi-dimensional Eulerian adaptive mesh refinement

(AMR) code, was used for the three-dimensional computations. It was developed and is currently supported by AX-Division at Lawrence Livermore National Laboratory (LLNL) [12]. There was a strong correlation between their experimental and numerical results, see Fig. 1.6.
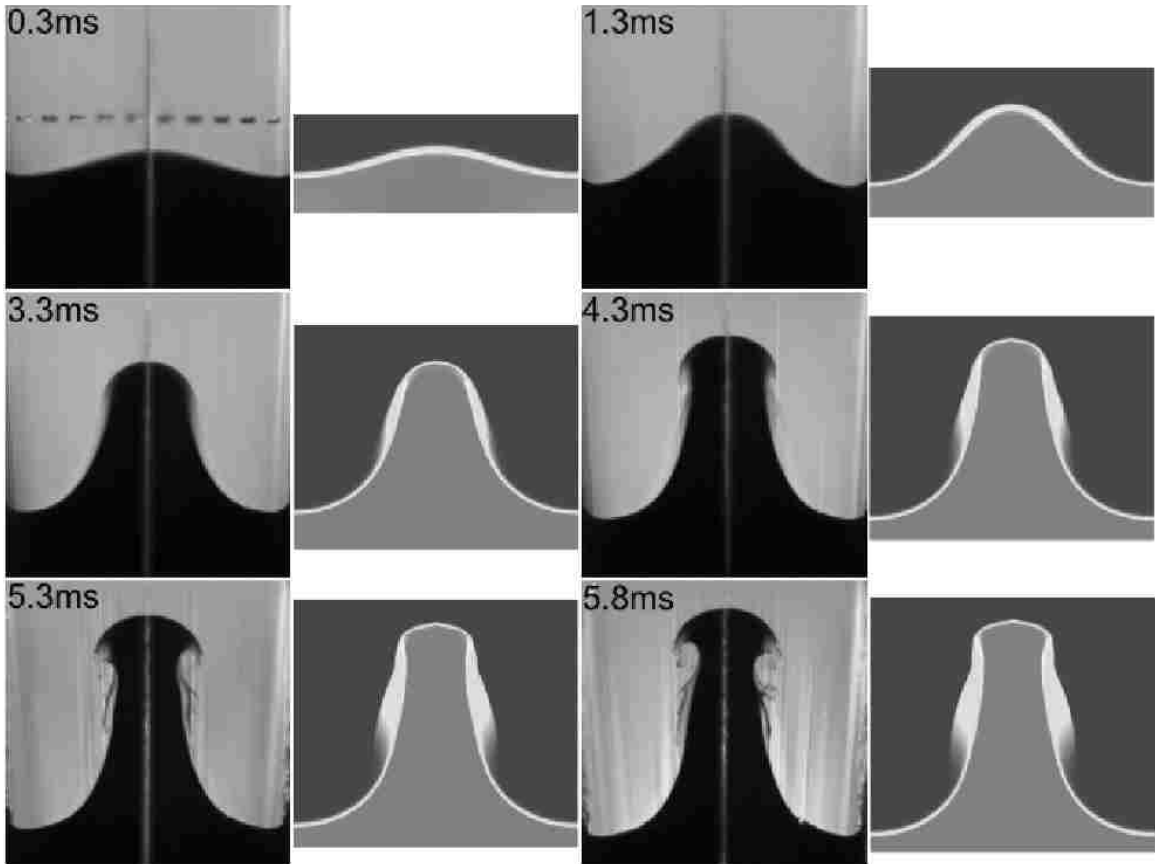
Figure 1.6: A sequence of PLIF images (diagonal slices) along with corresponding concentration maps obtained from the simulation. From Krivets et al. [12].

Since the resolution of that simulation was relatively low, the same degree of vortex roll-up was not quite achieved. However, the amplitude measurements showed excellent agreement between experiment and simulation, which illustrated a relative insensitivity of amplitude measurements to fine interface features [12]. Krivets et al. also noted that there is a dependence on the Atwood number to produce asymmetry in RM flows.

Spatially and temporally resolved experimental RMI studies were carried out by Rightley et al. [13, 14], Prestridge et al. [15], Vorobieff et al. [16], and Kumar et al. [17, 18]. In these studies, a variety of diffuse density interface geometries were subjected to a planar shock acceleration at M=1.2, with gas concentration and in some cases flow field velocity data collected and analyzed. These experiments revealed a variety of interesting behaviors, including the specifics of transition to turbulence [16] and the keen dependence of the flow evolution on the initial density distribution [18]. In all cases considered, however, the initial conditions were nominally two-dimensional.

As one can see from the reviewed literature, the state of the art in experimental studies of RMI flows was behind the computational work in two areas. First, there were relatively few works considering three-dimensional initial conditions (such as those produced by an oblique shock interacting with a cylindrical density interface). Second, the role of particles in RMI experiments was limited to passively following the flow as tracers for visualization, although Rightley et al. [14] mention that there is quantifiable particle lag, where particles do not follow the gas flow immediately after shock acceleration. The work described here is the first step in alleviating these shortcomings of the state of the art in experimental RMI studies. In the next chapter, a description of our experimental set up and diagnostic capabilities will be given, while the following chapter will describe the first experimental results for horizontal and oblique shock interactions with a particle-seeded heavy gas cylinder.

Chapter 2

Experimental Setup and Diagnostics

2.1 Overview

Our experimental setup consists of a shock tube which is constructed from 10.16 *cm* square 6061*T*6 Aluminum tubing with a 1.27 *cm* wall thickness. The tube is divided into four sections; the driver, driven, test, and run-off sections, see Fig. 2.1.

The driver section uses a circular 9.53 *cm* outer diameter tubing with a 1.27 *cm* wall thickness. The reason for using a circular driver section is simply to reduce high stress concentrations that are inherent in a square driver section. A 0.64 *cm*
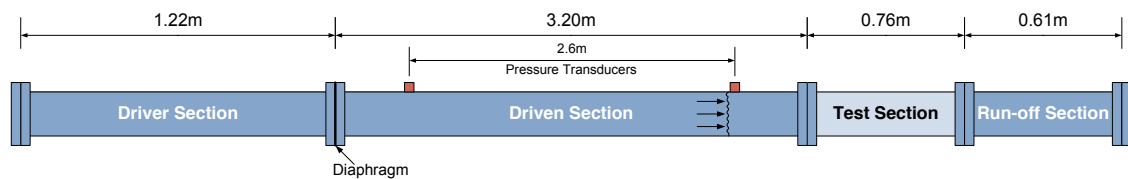

Figure 2.1: Diagram showing the layout of the shock tube and the individual sections.

diameter shaft positioned concentrically inside of the driver section has a puncturing device mounted on one end. The puncturing device consists of four mounted utility blades which puncture the diaphragm, initiating an experiment. The other end of the shaft is connected to an electronic solenoid which actuates the puncturing device. Attached to the driver section is the driven section which has two pressure transducers mounted at each end. The test sections are constructed from Lexan with a 1.27 *cm* wall thickness to provide transparency that allows for undistorted diagnostics of phenomena that occur during an experiment. There are multiple test sections used for injecting the SF_6 at angles of 0°, 15°, and 30° from vertical. The fact that the shock tube has the ability to be tilted, allows us to conduct experiments involving 3D initial conditions and oblique shock wave interactions with a droplet-seeded gas cylinder.

2.2 Injection System

The injection system consists of a tank of SF_6 which is fed into a chamber where it is stored temporarily during experiments. A smoke machine sitting on top of the chamber, when activated by push-button control, seeds the SF_6 with glycol droplets allowing us to visualize the gas cylinder when it is injected into the test section, see Fig. 2.2 and Fig. 2.3. From the chamber, the seeded mixture is fed via a Teflon tube approximately 6 *mm* in diameter, into a nozzle that is fixed in the top of the test section. The primary reason for using Teflon is that it is resistant to acetone which is used for fluorescence, and will not deteriorate over time. The gas cylinder exits the bottom of the test section through a hole and vents to atmosphere.

After several experiments, the chamber temperature begins to rise due to the high temperature of the entering glycol droplets. This causes some turbulence in the gas cylinder which makes it difficult to extract data from the resulting images. Adding a concentric flow of air around the gas cylinder would act to minimize turbulence.
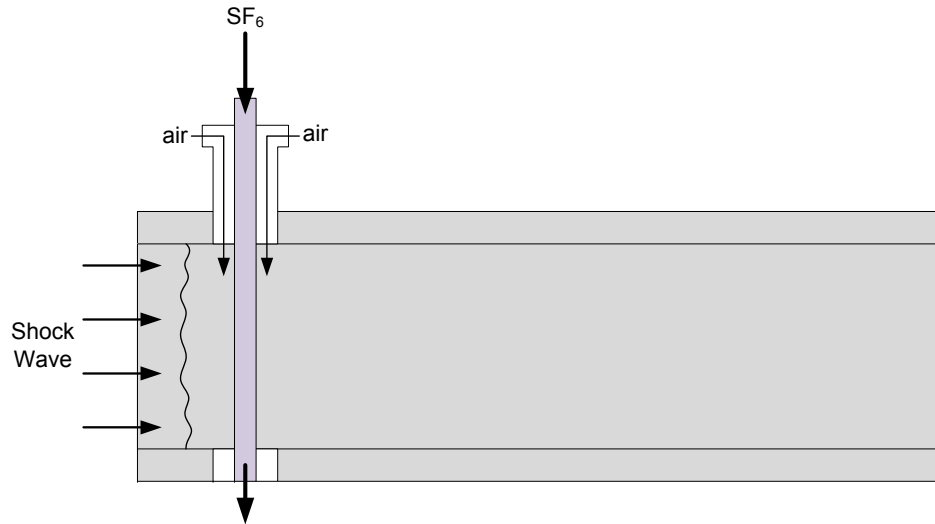
Figure 2.2: Diagram showing the injection system with co-flow implemented for the planar shock wave experiments.

We integrated a two-phase solution by installing a co-flowing cylinder of air into our injection nozzle as well as adding ice to the chamber. This acts to cool the SF_6 as it enters the chamber and maintains an overall lower temperature inside the chamber. Our white light sources also cause the test section to rise in temperature which can cause undesirable effects, including buoyancy. With this modification we were able to increase the stability of the cylinder and mitigate the interference of turbulence in our initial conditions.

2.3   Diagnostics

An Imacon 200 ultra-high speed digital camera is used to capture the shock wave interaction with the gas cylinder, see Fig. 2.4 [19]. The Imacon 200 uses multiples of intensified CCD modules providing simultaneous framing and streak recording
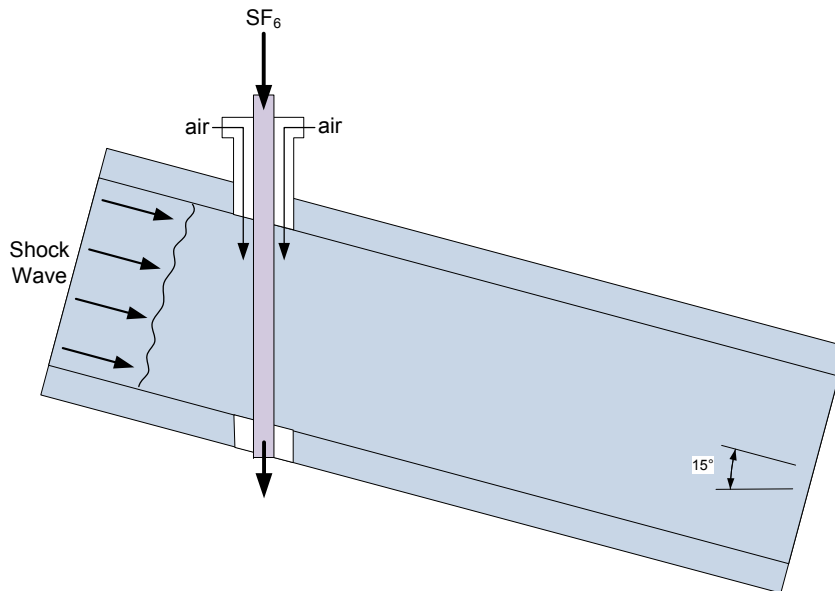
Figure 2.3: Diagram showing the injection system with co-flow implemented for the oblique shock wave experiments.

through a single optical axis. The camera has a maximum frame rate of 200 million frames per second from which we can capture 14 exposures at maximum resolution. High spatial and temporal accuracy make the Imacon 200 an ideal system for capturing our images. The camera is controlled via a dedicated computer with software that allows us to manipulate the way the camera performs. Illumination is provided via two Fastax floodlights originally designed for ultra-high speed cinematography. Unlike conventional floodlights, they do not exhibit brightness fluctuations with time. In addition to the floodlights, four LED arrays are use. Each LED array consists of approximately 100 individual LEDs.

The camera receives a trigger from the first of two pressure transducers. The transducers are mounted in the driven section, 2.6 m apart. Analysis of the signals from the pressure transducers allows us to verify the theoretical Mach number as well as diagnose any problems that may have occurred during an experiment. A

Figure 2.4: DRS Imaging Imacon 200 high-speed camera [19].

delay generator is also used to compensate for the time it takes the shock wave to travel the distance of the driven section into the proper location of the test section, see Fig. 2.5 [20].

2.4   Additional Capabilities

In addition to the Fastax floodlights and four LED arrays, two 532 nm (used for particle visualization) and one 266 nm (used for gas phase Planar Laser Induced Fluorescence (PLIF)) double pulsed lasers can be used for visualization purposes. The camera is oriented so that a side view and top view can be seen simultaneously in each frame see Fig. 2.6.

Another feature of our injection system is the use of an inline filtering flask containing acetone. SF_6 is fed into the filtering flask via a glass pipette with its end submerged in the acetone. The bubbling that occurs seeds the exiting SF_6 with acetone particles that cause the gas cylinder to fluoresce under laser illumination. A combination of optical lenses, mirrors, and filters will allow us to employ planar laser
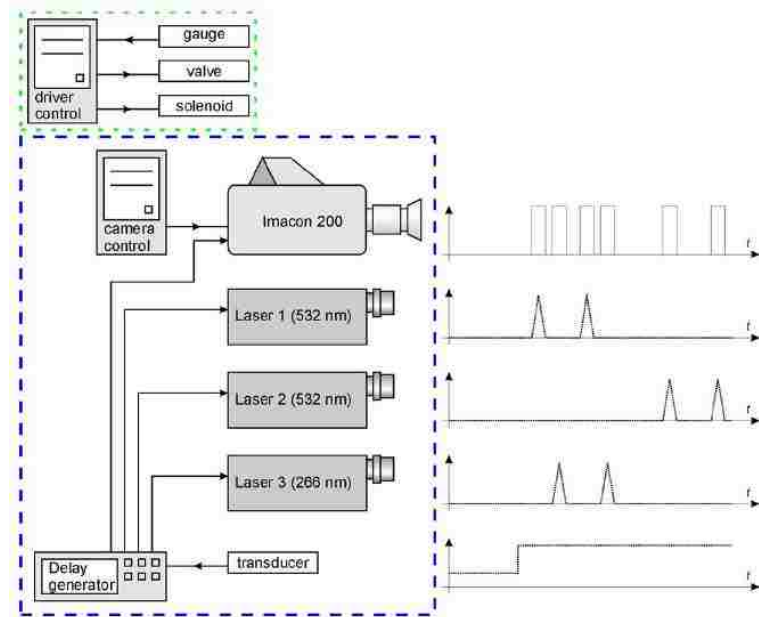
Figure 2.5: Schematic showing how the camera, delay generator, lasers, and transducers are configured. For details refer to Chavez et al. [20].

induced fluorescence (PLIF). Manipulation of laser beams enables us to visualize a slice of the gas cylinder with which the shock wave interacts. Also, there are other features of the flow that are slightly visible in our results from the Imacon 200 that can be analyzed in more detail by using laser diagnostics in addition to other visualization techniques.

Figure 2.6: Diagram showing the orientation of Imacon 200 relative to test section (left) and an individual frame representative of typical experimental results (right).

Figure 2.7: Raw frames without acoustic pre-shock.

2.5   Acoustic Pre-shock

In our preliminary experiments, we were able to capture the cause of acoustic pre-shock. The pre-shock was observed by earlier experimenters Kumar et al. [18]. It manifested itself as an acoustic perturbation that distorted the initial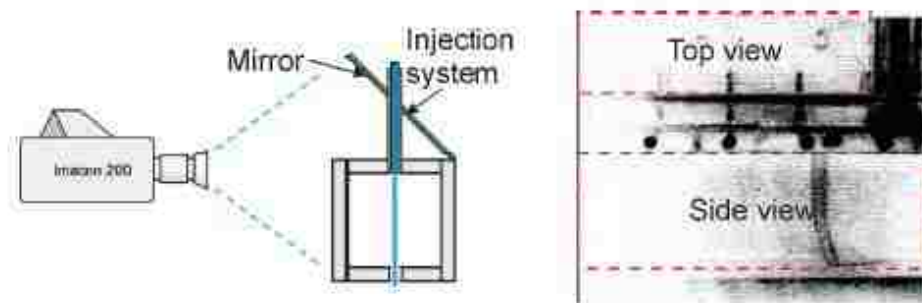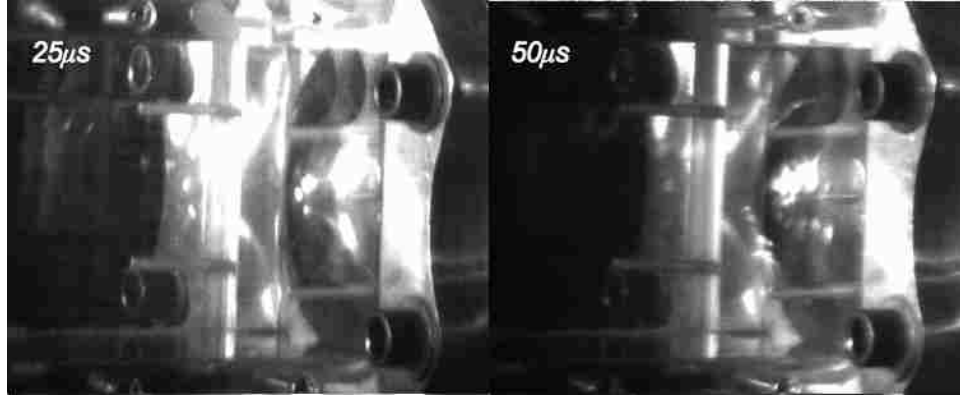 conditions prior to the arrival of the main shock wave, but its origins were not understood. With our test section attached directly to the driver section, we triggered the camera from the switch that is used to actuate the puncturing device. With the driver section pressurized, we activated the puncturing device and with two diaphragms in place we were able to see the first diaphragm get punctured and second diaphragm actually bulge and burst before the puncturing device could reach it. This late rupture of the second diaphragm is the cause of acoustic pre-shock, see Fig. 2.8. To avoid acoustic pre-shock, we experimented with different types of diaphragm materials. It seemed that the elasticity was too high in the diaphragm sheets that we were using. We used some more brittle sheets and this seemed to provide a more stiff rupture of the diaphragms which eliminated the acoustic pre-shock. Figs. 2.7 and 2.8 both consist of two consecutive frames showing an experiment without acoustic pre-shock as well as showing an experiment with acoustic pre-shock.

The elapsed time between the frames was 0.025 *ms*. In Fig. 2.7, the first frame
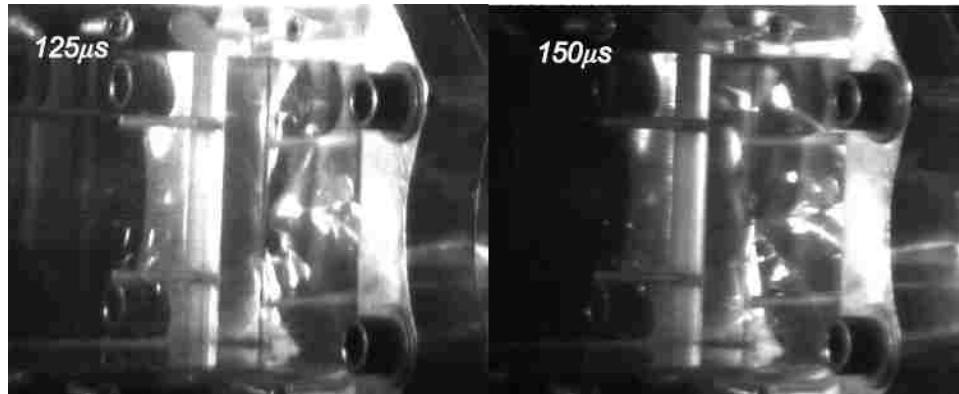
Figure 2.8: Raw frames with acoustic pre-shock.

(left) and the second frame (right) were taken at $t = 0.025\ ms$ and $t = 0.050\ ms$, respectively. The puncturing device effectively ruptures both diaphragms from one frame to another. In Fig. 2.8, the first frame (left) and the second frame (right) were taken at $t = 0.125\ ms$ and $t = 0.150\ ms$, respectively. The first frame shows the outer diaphragm bulging before it bursts due to yielding, not from being punctured. The additional time that it took for the diaphragms to rupture completely was due to the bulging of the second diaphragm. Acoustic pre-shock was causing problems with timing since it introduced an inconsistency into our system. By changing the diaphragm material we were able to avoid acoustic pre-shock.

Chapter 3

Results of Experiments

We will present the results from experiments conducted at Mach numbers of 1.2, 1.9, and 2.4, with the shock tube at an incline of 15° from the horizontal. However, for the horizontal experiments results will only be presented for Mach numbers of 1.9 and 2.4 simply due to lack of data. We were still able to confirm earlier observations as well as reveal new features of the flow. The analysis of the oblique shots allowed us to gain information about how an oblique shock wave interacts with the gas cylinder. It was possible to analyze a rotation of the gas cylinder since some "straightening" occurs immediately upon the shock wave interaction. This is discussed further in section 3.2.

3.1   Horizontal Experiments

Experimentation began with the shock tube oriented in a horizontal position, producing planar shock wave interactions with the SF_6 gas cylinder. Using $ImageJ$, an image analysis software, we were able to extract data such as the piston velocity, development of the counter-rotating vortex pair, as well as observe differences in these quantities when compared at different Mach numbers. The Mach 2.4 planar
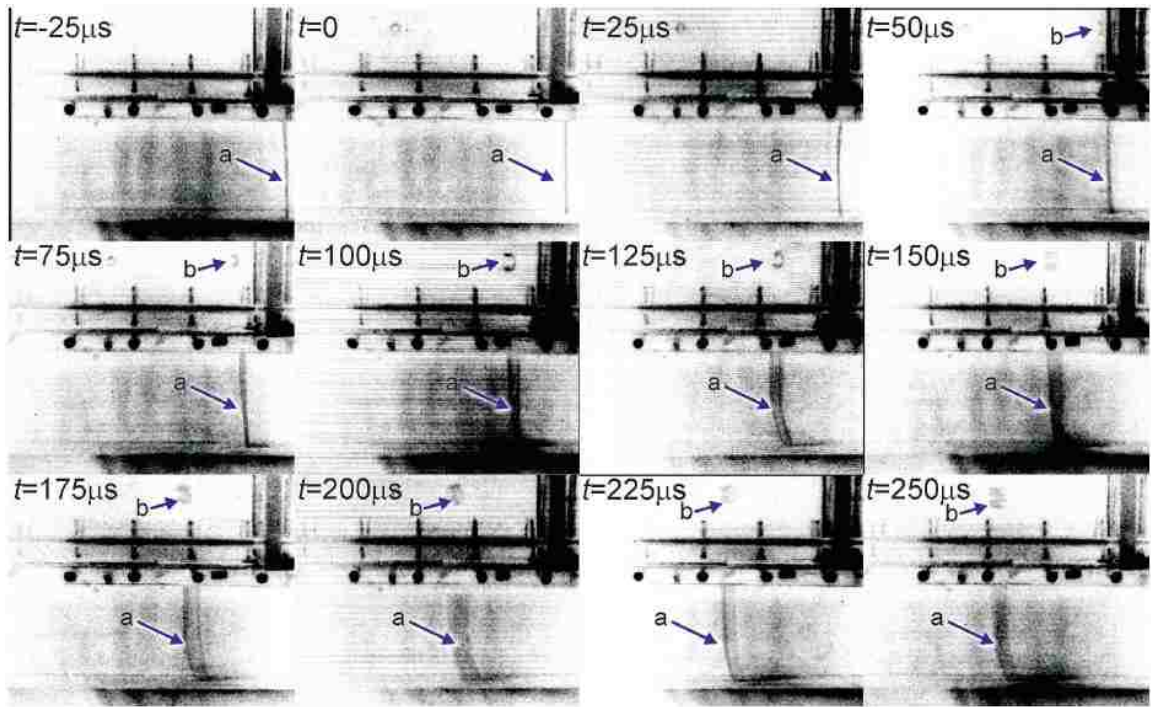
Figure 3.1: Processed image sequence, inverted and contrast-enhanced, Mach 2.4 acceleration of SF_6 gas cylinder with shock tube in the horizontal orientation.

shock wave acceleration of the gas cylinder embedded in air is shown as an example of our results, see Fig. 3.1. Labels in the top left corner of each frame denote time t, with $t = 0$ corresponding to the shock arriving at the cylinder. Each frame shows a combination of the top (above) and side (below) view. Arrows with the index 'a' denote the location of the side view of the gas cylinder in each frame; arrows with the index 'b' point to the corresponding top view. Note that in the first three images, the top view is completely obscured by the injection nozzle, and in the fourth image, it is partially obscured.

The injection nozzle was positioned vertically in the test section. This configuration allowed us to study phenomena that are inherent with the normal acceleration of a gas cylinder composed of a heavy gas embedded in a lighter gas. Horizontal experiments allowed us to confirm observations made in earlier studies of the acceleration of an SF_6 cylinder embedded in air. The evolution of the Richtmyer-Meshkov

Instability can be clearly seen in both the top and side views. Once the shock accelerates the gas cylinder, the counter rotating vortex pair begins to develop. Also, glycol droplets from the gas cylinder are advected into the top and bottom boundary layers after the shock wave passes.

Analysis of the pressure traces from each experiment enabled us to confirm the speed of the shock wave and verify that we were indeed reaching a particular Mach number. Further image analysis gave a piston velocity from each experiment which was verified through hand calculations using fundamental gas dynamics equations. Further analysis and experiments are planned to study the development of the boundary layer in addition to other instabilities. This, however, will require the implementation of our laser diagnostic methods both to increase the resolution of our results and allow us to take more accurate measurements.

By analyzing the images from each experiment, we are able to calculate a piston velocity simply by measuring the distance in which the gas cylinder travels over the time span of the captured frames. Since we know the dimensions of our test section, we can set a scale in the image analysis software causing all of the measurements to have the particular units in which we specify. We document the frame interval of each experiment to keep track of the total amount of elapsed time. By plotting the translation of the gas cylinder versus time, a piston velocity can be calculated from the slope of the curve for a particular Mach number, see Fig. 3.2.

There was little error between experimental piston velocities and theoretical piston velocities. A linear regression on each curve shows that the velocity of the gas cylinder is nearly constant at each Mach number after shock acceleration. For each experiment, measurements were taken from both the top and the side views. From the side view, velocity is the main parameter that is extracted. However, from the top view, measurements are made to quantify how the counter-rotating vortex pair is developing over time. Both width (in the direction normal to the streamwise) and streamwise span measurements are taken and plotted against time, see Fig. 3.3
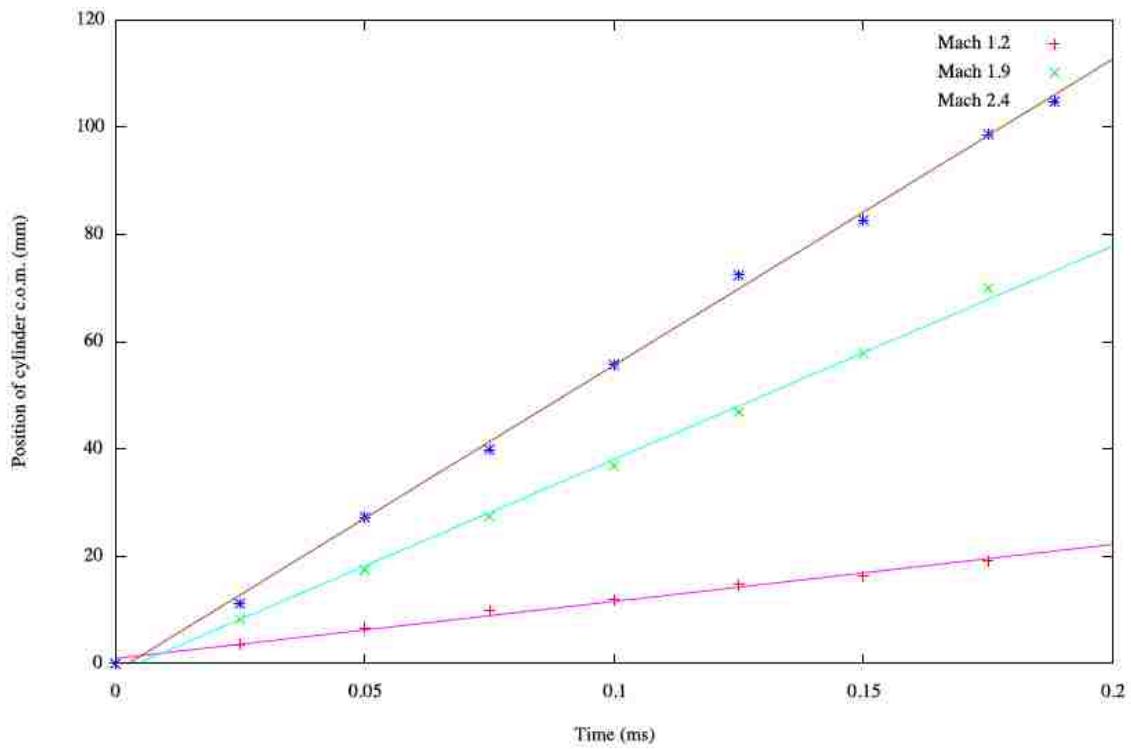
Figure 3.2: Translation of the center of mass of the gas cylinder from $t = 0 \ ms$ to $t = 0.175 \ ms$ for Mach numbers 1.2, 1.9, and 2.4 with shock tube in horizontal orientation.

and Fig. 3.4. When compared to the results others have obtained from similar experiments [16], our counter-rotating vortex pair develops in a very similar manner, with the geometrical feature growth consistent with hyperbolic sine-like models that were developed for fitting data from earlier studies [14]. While these trends are the same for all Mach numbers, higher values of the Mach number result in faster initial growth and slightly larger overall size.

When comparing width and span measurements between various experiments, it was determined there was a small variation (± 1.5 mm), likely due to initial condition fluctuations. This is represented by the error bars in the width and span plots. In the width versus time plot from $0 \ ms$ to approximately $0.05 \ ms$, it can be seen that the development of the counter-rotating vortex pair begins at a rate that is substantially
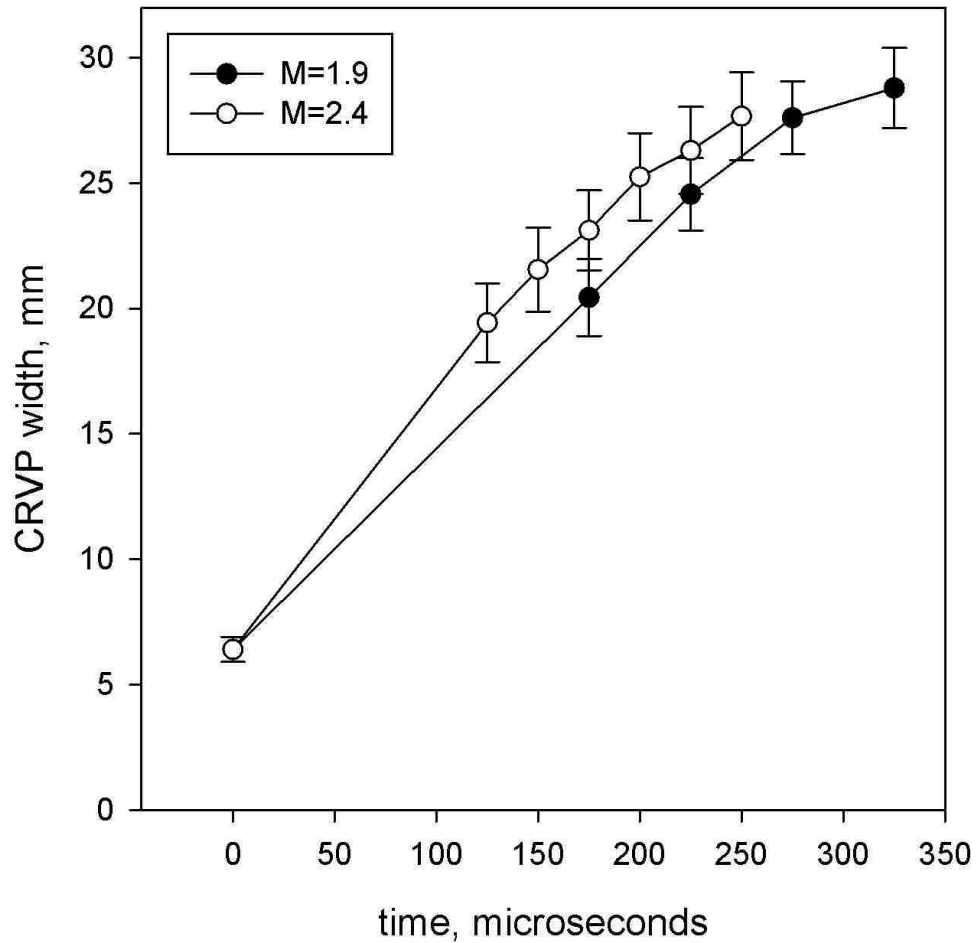
Figure 3.3: Width (in the direction normal to the streamwise) of counter-rotating vortex pair versus time with shock tube in the horizontal orientation.

higher than the rest of the development beyond 0.05 ms. Initially, when the shock wave interacts with the gas cylinder, much of the growth of the instability takes place toward the beginning of the total development. Beyond 0.05 ms the counter-rotating vortex pair continues to grow in width but at a much slower rate. Similar trends can be observed for the span. These effects are more dramatic, of course, at higher Mach numbers. An interesting observation when comparing the width plot from horizontal shots to the width plot from vertical shots, is that in the inclined orientation the width of the counter-rotating vortex pair develops at a much steadier and gradual rate than that of the horizontal orientation. This is discussed in the next section.
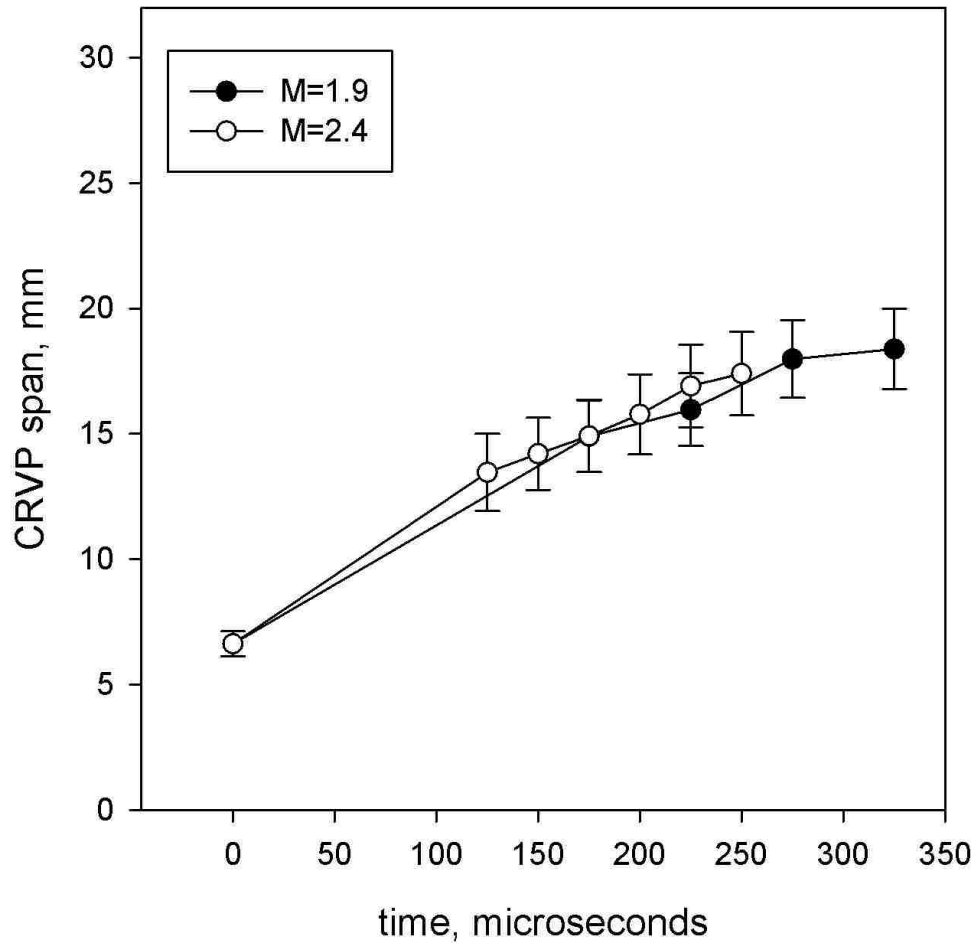
Figure 3.4: Span (in the streamwise direction) of counter-rotating vortex pair versus time with shock tube in the horizontal orientation.

3.2   Oblique Experiments

For the experiments involving oblique shocks, the shock tube was inclined at an angle of 15° from the horizontal. This configuration creates the scenario of an oblique shock wave accelerating a heavy gas cylinder while of course the shock is still traveling normal to the longitudinal axis of the shock tube, see Fig. 3.5.

Fig. 3.5 shows a Mach 2.4 shock acceleration of an SF_6 cylinder embedded in air. The angle between the plane of the shock and the central axis of the cylinder is 15°. Each frame shows a combination of top (above) and side (below) view. The

Figure 3.5: Processed image sequence, inverted and contrast-enhanced, Mach 2.4 acceleration of SF_6 gas cylinder with shock tube inclined 15° from horizontal.

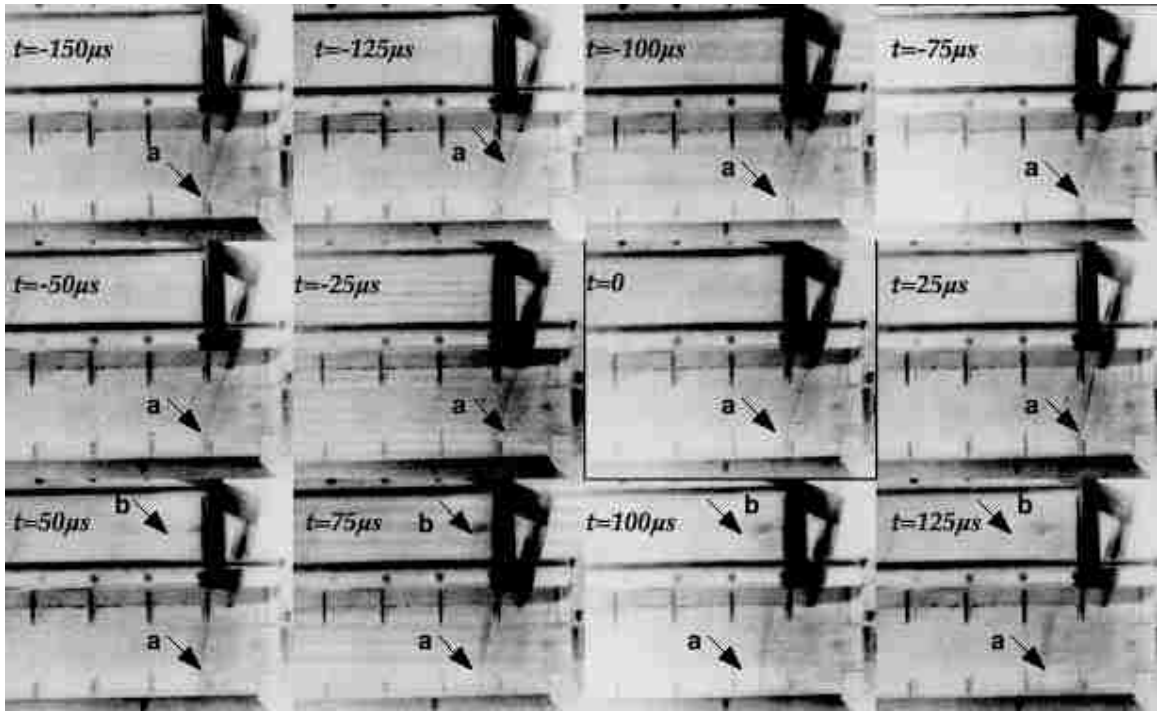image timings in the first twelve frames are identical to those in Fig. 3.1 with a 25 microsecond interval between all the frames. Note the advection of the cylinder material into the top boundary layer, particularly visible in the top view in the last two frames ($t = 0.275$ ms and $t = 0.300$ ms). The piston velocities of the oblique experiments were verified in the same way as the horizontal experiments.

The rotation of the cylinder may allow us to calculate rough angular velocities (and thus circulations). We plan to study this rotation in more detail, and make correlations between the interaction of the pressure and density gradients. Experiments conducted in the inclined orientation produce results that are substantially different than those from the horizontal experiments. These differences will be discussed in more detail in the next section. The major difference, however, is in the flow evolution in the plane of the side view. When the shock wave accelerates the gas cylinder, a slight rotation, or straightening, of the cylinder occurs. The rate at
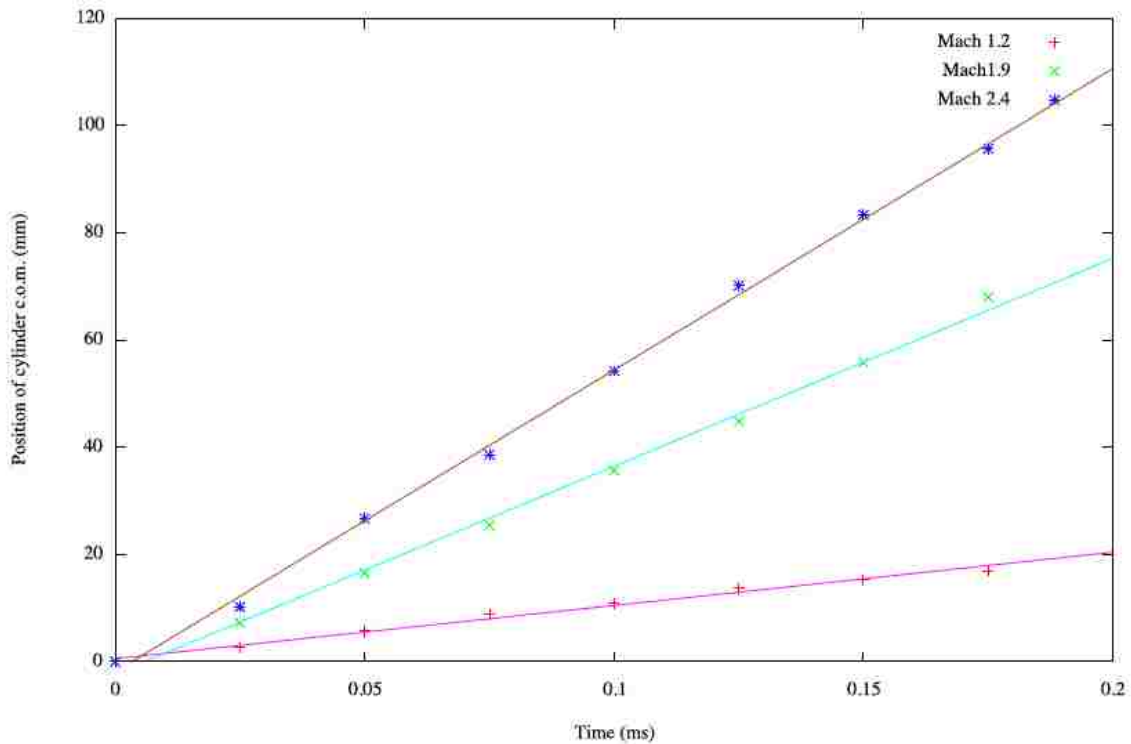
Figure 3.6: Translation of the center of mass of the gas cylinder from $t = 0 \ ms$ to $t = 0.175 \ ms$ for Mach numbers 1.2, 1.9, and 2.4 with shock tube in the inclined orientation.

which the cylinder rotates, as well as the extent to which the cylinder rotates, varies considerably with the Mach number, see Fig. 3.7.

Fig. 3.7 shows that for a particular Mach number there is also a particular rate of rotation as well as a terminal angle about which the gas cylinder tends to settle. The increase in Mach number decreases the "settling time" of the rotation of the gas cylinder, beyond which further angle changes cannot be resolved. While some of the early-time rotation can be attributed to the medium (including the cylinder material) being compressed behind the shock front, effects of such compression on the angle should be nearly instantaneous. However, we observe gradual changes in the angle of the cylinder, which may be attributable to some three-dimensional baroclinic effect. We plan to analyze these effects more in future experiments.
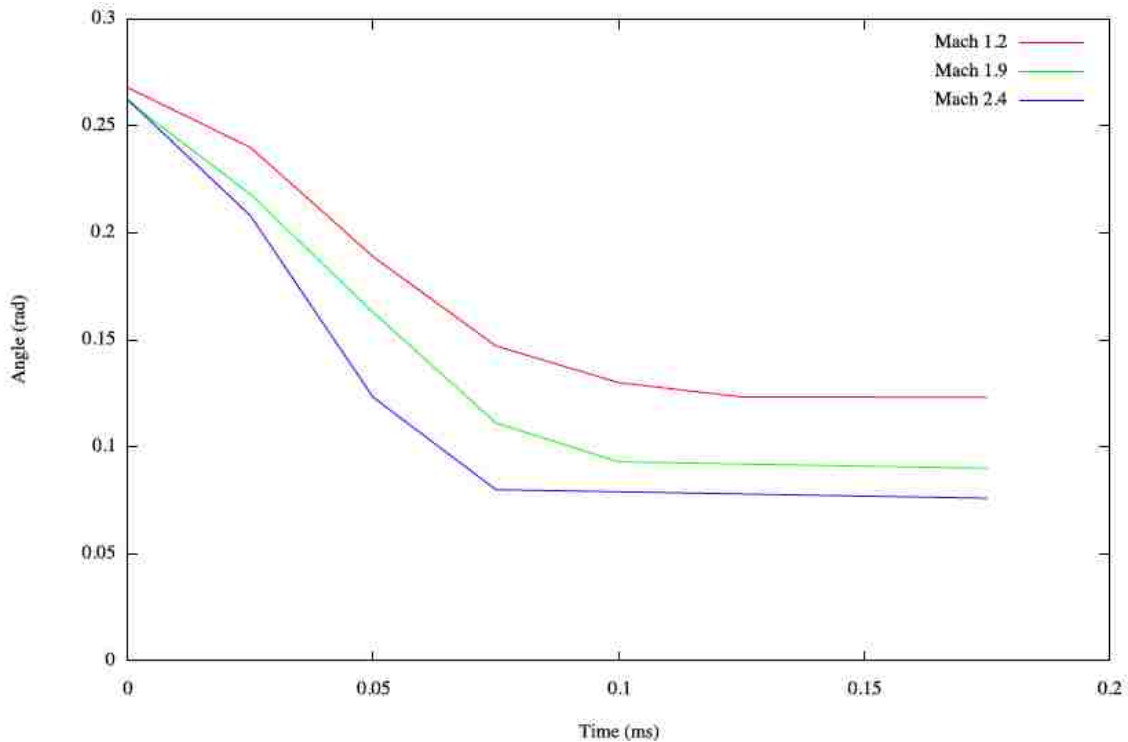
Figure 3.7: Change in the angle of the gas cylinder relative to the shock front versus time.

In Fig. 3.8, width measurements are plotted versus time and in Fig. 3.10, span measurements are plotted versus time. The growth rate of the width for the tilted cylinder is quantifiably behind that for the straight cylinder at each corresponding Mach number. The span measurements for the tilted experiments involve a larger uncertainty due to variation in the extent of the gas cylinder that was taken into account. These measurements were actually taken from the side view of our images. From the top view in the inclined experiments, it is not possible to get span measurements since we are no longer looking down the axis of the gas cylinder and the span of the CRVP is slightly obscured. The span measurements are nominally smaller in the inclined experiments than they are in the horizontal experiments, again, due to three-dimensional effects. It seems that the difference in initial conditions somewhat inhibits the overall increase in width of the counter-rotating vortex pair. One of the

Figure 3.8: Width (in the direction normal to the streamwise) of the counter-rotating vortex pair versus time with shock tube in the inclined orientation.

reasons for this may be due to the way the shock wave interacts with the gas cylinder. In the planar shots, all of the energy that is dispersed in the gas cylinder manifests itself through the growth of the counter-rotating vortex pair. In the oblique shots, some of this energy is dispersed in the development of the counter-rotating vortex pair, but some of it also contributes to the rotation of the gas cylinder in the third dimension. Correspondingly, the additional angle between the direction of the shock and direction of the interface has to be taken into consideration when computing the baroclinic vorticity component normal to the plane of the top view, thereby reducing that component.
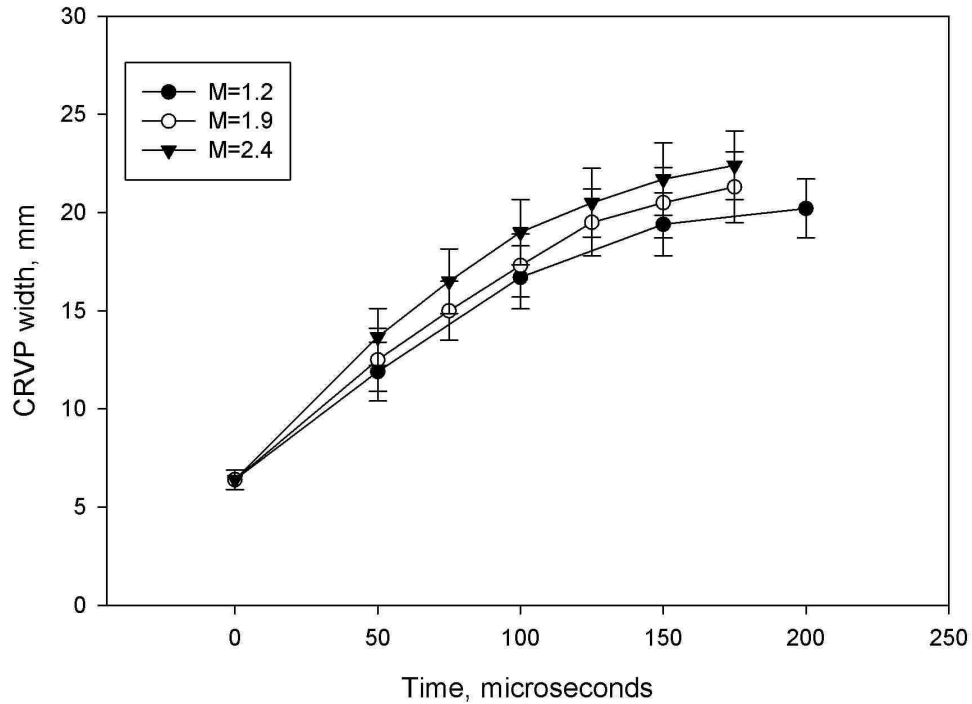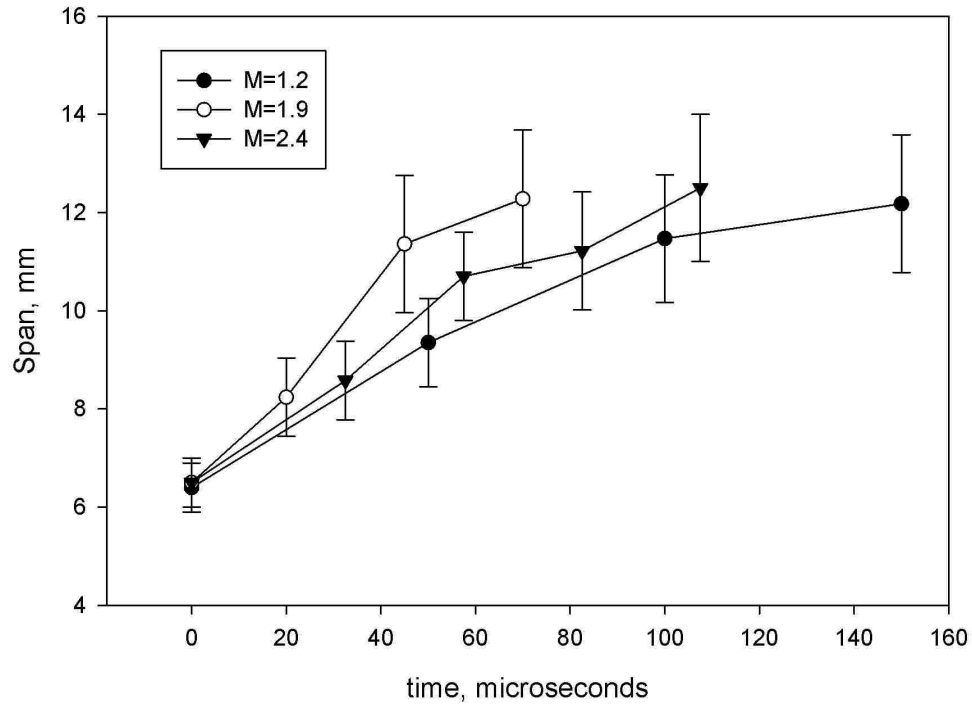
Figure 3.9: Span (in the direction normal to the streamwise) of the counter-rotating vortex pair versus time with shock tube in the inclined orientation.

3.3 Observations

In a typical experiment involving either a planar or oblique orientation of the shock tube, we extracted some of our data from a series of images produced by our Imacon 200. The side view and top view of the test section both reveal different mixing phenomena and flow instabilities. In planar experiments, the side view shows the acceleration of the gas cylinder by the shock wave and allows us to visualize the advection of the glycol droplets into the upper and lower boundary layers. Since the initial conditions are symmetric, it makes sense that advection would take place symmetrically. The gas cylinder maintains a relatively straight orientation as the gas cylinder is accelerated.

After several frames (since these frames are obscured by the mirror brackets and injection nozzle), in the top view we start to see the development of the counter-

rotating vortex pair. It develops in a similar way in both planar and oblique experiments, but the size to which it grows is not the same. Overall, the width and span of the counter-rotating vortex pair were nominally smaller in the oblique experiments than they were in the planar experiments. In oblique experiments, the side view shows not only the acceleration of the gas cylinder, but it also shows the partial realignment of the gas cylinder with the plane of the shock wave. It seems that the straightening of the gas cylinder inhibits the development of the width of the counter-rotating vortex pair. The width was approximately 5 *mm* less in the oblique experiments than it was in the planar experiments. Advection in the oblique experiments seemed to occur preferentially along the top wall of the test section due to the misalignment of the pressure and density gradients, which would be consistent with an effect of baroclinic vorticity in the plane of the side view.

With increasing Mach number, similar effects were observed in both planar and oblique experiments. Obviously piston velocity increased with increasing Mach number, but in the oblique experiments, the rate at which the gas cylinder was partially realigned with the shock front increased as well. The overall amount of straightening that took place also increased with Mach number, causing the gas cylinder to become more closely aligned with the shock front as we increased the shock speed. Furthermore, a higher concentration of glycol droplets was advected into the boundary layers as the Mach number increased. This was observed by the decrease in transparency of the material that was advected into the boundary layer.

The main difference between the horizontal and oblique experiments is in the initial conditions; more specifically, the angle of injection. When the shock wave arrives and interacts with the cylinder, it can be seen in our images that material is advected into the boundary layers along the insides of the test section. In the horizontal experiments, there is material that is advected into both the top and bottom walls of the test section. This is simply due to the symmetry that exists in the initial conditions. Since the pressure and density gradients are aligned in the horizontal experiments, there is no rotation of the cylinder when the shock wave
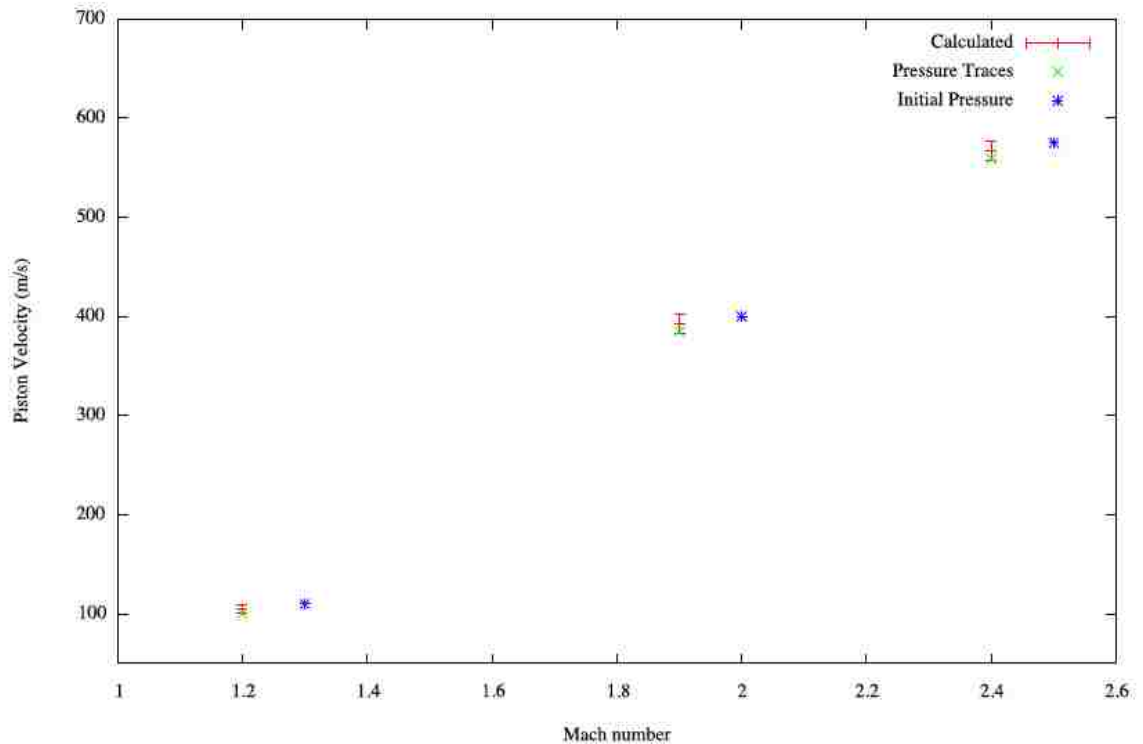
Figure 3.10: Piston velocity versus Mach number.

arrives. This is not the case, however, in the inclined experiments.

With 3D initial conditions, i.e. the cylinder being injected at 15° from the shock front, the pressure and density gradients are no longer aligned. Now, the cross product of the two gradients has a non-zero value, producing vorticity of opposing signs on the leading and trailing interfaces of the cylinder. The cylinder rotation due to compression and possibly 3D baroclinic effects causes material to be advected primarily into the boundary layer along the top wall of the test section. This is why the gas cylinder material is being advected into both the top and bottom boundary layers (Fig. 3.1), or just the top boundary layer(Fig. 3.5).

In Fig. 3.10, the average piston velocities from both horizontal and inclined experiments are plotted against the corresponding Mach number. There are three different series of piston velocities. The first series titled *"Calculated"*, are the piston veloci-

ties that result from computing the Mach number based on the piston velocity. The error was calculated using a linear fit on each curve from Figs. 3.2 and 3.6. This error is represented through the use of error bars on the *"Calculated"* series. The next series, titled *"Pressure Traces"* shows the piston velocities computed for the same experiments for a particular Mach number as determined by the data from our pressure transducers. Knowing the distance between the two pressure transducers, we can analyze the data and divide this distance by the time that it took the shock wave to travel from one transducer to the other. This gives us a shock speed from which we can calculate a Mach number and the resulting piston velocity. These piston velocities ended up within the uncertainty margin of the *"Calculated"* series. The third and final series titled *"Initial Pressure"* was calculated by using the initial conditions in the pressurized section of the shock tube (driver pressure) recorded in the experiments. This calculation showed that we should be achieving a higher Mach number than we actually were for a given driver pressure. This makes sense since we have losses that occur during an experiment. Some of these losses include flow restriction caused by the puncturing device, imperfect rupture of the diaphragm material, and slight error in the equipment we use to monitor the pressure in the driver section at any given time. Overall there is good agreement between theoretical and experimental piston velocities.

Chapter 4

Conclusions and Future Work

4.1 Conclusions

Many studies have been performed to diagnose perturbations at a density interface between two fluids subjected to a normal shock wave, but few studies have yet been done and well understood in diagnosing the formation and evolution of instabilities that occur when a gas cylinder is accelerated by an oblique shock wave. The results of our experiments show that baroclinic vorticity in three dimensions does play a role in the rotation of the gas cylinder in the vertical plane parallel to the streamwise direction. It is very likely that more work will be done in this area and progress will be made toward understanding and discovering new phenomena associated with oblique shock wave interaction with a droplet seeded gas cylinder.

4.2 Future Work

Future experiments will lead to more detailed analysis of shock wave interactions with a gas cylinder. The level of detail in our data will be increased drastically due to laser illumination and more accurate tracking of fluorescent particles seeded in the

gas cylinder. Additionally, various substances added to the SF_6 chamber may lead to a more strongly defined gas cylinder, increasing visibility and contrast in our image sequences. The shock tube is engineered to produce shock wave speeds up to Mach 4.1. Future experiments are planned at various Mach numbers for both horizontal and inclined shock tube orientations. Theoretical shock velocities are calculated so that we can predict and set our diagnostic system timings in order to capture the event.

An indirectly observed event occurred during the preparation for our experiments. While filling our holding chamber with SF_6, we allow the fog machine to heat up so that the chamber can be filled with glycol droplets. When the fog is pumped into the chamber, it briefly sits on top of the SF_6 and begins to slowly develop into a Raleigh-Taylor instability in three dimensions. When properly illuminated, there are some very interesting structures that form during the pumping of glycol droplets into the chamber. We plan on filming this event and analyzing the results to benchmark any new behaviors that are observed.

The droplets in the gas cylinder cause it to take on a light gray color, which allows for sufficient visualization with our current diagnostic setup. However, experimentation with different chemicals added to our gas chamber could prove to increase the visibility of the gas cylinder. Furthermore, adding different chemicals to the filtering flask in our injection system, causing the SF_6 to be seeded with that particular chemical, will allow for different intensities of fluorescence when utilizing laser diagnostic techniques.

Currently the end of the shock tube is open to atmosphere, allowing the shock wave to exit through the end of the run-off section. There are two different end flanges that can be bolted onto the run-off section. One is a solid flange that simply seals the entire shock tube. The other is a flange that is composed of two halves that when bolted to the run-off section, house a circular piece of optical glass. This visualization window allows for laser illumination that is collinear with the longitudinal axis of

the shock tube. Mainly these two flanges will be used for studies of re-shock, which occurs when the incident shock wave is reflected back through the path in which it initially traveled. We will also study the effects of rarefaction waves which are associated with an area of low pressure following the shock wave.

Another experimental configuration we plan to explore in the future is to orient the shock tube at -15° from the horizontal with the corresponding test section installed. In this scenario, the initial conditions will be opposite of those in the inclined experiments that were previously conducted. The shock wave will first interact with the bottom of the gas cylinder instead of the top of the gas cylinder. These experiments could reveal new instabilities or other interesting phenomena. We will analyze the angular velocity of the cylinder once it is accelerated by the shock and then proceed to compare the results to those from the previously conducted inclined experiments. Moreover, we will make correlations between which surfaces of the test section the glycol droplets are advected and the orientation of pressure and density gradients. In the previously conducted inclined experiments, the gas cylinder droplets were advected into a boundary layer along the upper inside wall of the test section. In the horizontal experiments the glycol droplets were advected into the boundary layers along the top and bottom walls of the test section. It will be interesting to see what happens when the shock tube is oriented at -15° from the horizontal. It is possible that new phenomena could result from conducting experiments at angles other than 0° and 15° from horizontal.

We have multiple test sections that are each designed for experiments conducted at a particular angle. Ultimately, we would like to have data for experiments conducted with combinations of different shock tube orientations and different test sections. Furthermore, we intend to submit proposals for additional funding to organizations who are interested in any of the various applications in which this work entails.

References

[1] K. O. Mikaelian. Oblique shocks and the combined rayleigh-taylor kelvin-helmholtz, and richtmyer-meshkov instabilities. *Physics of Fluids*, 6(6):1943–1945, June 1994.

[2] L.D. Landau and E.M. Lifshitz. *Fluid Mechanics*. Butterworth-Heinemann, 2nd edition, 1987.

[3] R.D. Zucker and O. Biblarz. *Fundamentals of Gas Dynamics*. John Wiley & Sons, Inc., 2nd edition, 2002.

[4] S. Elghobashi. Particle-laden turbulent flows: direct simulation and closure models. *Applied Scientific Research*, 48(3-4):301–314, October 1991.

[5] A. Palekar, P. Vorobieff, and C. R. Truman. Two-dimensional simulation of a shock-accelerated gas cylinder. *Progress in Computational Fluid Dynamics*, 7(8):427–438, 2007.

[6] R. D. Richtmyer. Taylor instability in shock acceleration of compressible fluids. *Communications of Pure and Applied Mathematics*, 13:297–319, 1960.

[7] E. E. Meshkov. Instability of the interface of two gases accelerated by a shock wave. *Fluid Dynamics*, 4(5):151–157, September 1969.

[8] X. Yang, I. Chern, N. J. Zabusky, R. Samtaney, and J. F. Hawley. Vorticity generation and evolution in shock-accelerated density-stratified interfaces. *Physics of Fluids*, 4(7):1531–1540, July 1992.

[9] R. Samtaney and N. J. Zabusky. On shock polar analysis and analytical expressions for vorticity deposition in shock-accelerated density stratified interfaces. *Physics of Fluids*, 5(6):1285–1287, 1993.

[10] F. Utheza, R. Saurel, E. Daniel, and J. C. Loraud. Droplet break-up through an oblique shock wave. *Shock Waves*, 5(5):265–273, February 1996.

References

[11] J. H. S. Lee and D. L. Frost. Steam explosions - major problems and current status. Springer, 1987.

[12] V.V. Krivets, C.C. Long, J.W. Jacobs, and J.A. Greenough. Shock tube experiments and numerical simulation of the single mode three-dimensional richtmyer-meshkov instability. *Shock Waves*, pages 1205–1210, July 2007.

[13] P. M. Rightley, P. Vorobieff, and R. F. Benjamin. Evolution of a shock-accelerated thin fluid layer. *Physics of Fluids*, 9(6):1770–1782, 1997.

[14] P. M. Rightley, P. Vorobieff, R. Martin, and R. F. Benjamin. Experimental observations of the mixing transition in a shock-accelerated gas curtain. *Physics of Fluids*, 11(1):186–200, 1999.

[15] K. Prestridge, P. Vorobieff, P. M. Rightley, and R.F. Benjamin. Validation of an instability growth model using particle image velocimetry measurements. *Physical Review Letters*, 84(19):4353–4356, 2000.

[16] P. Vorobieff, N.-G. Mohamed, C. Tomkins, C. Goodenough, M. Marr-Lyon, and R. F. Benjamin. Scaling evolution in shock-induced transition to turbulence. *Physical Review Letters*, 68:065301.1–065301.4, 2003.

[17] S. Kumar, G. Orlicz, C. Tomkins, C. Goodenough, K. Prestridge, P. Vorobieff, and R. Benjamin. Stretching of material lines in shock-accelerated gaseous flows. *Physics of Fluids*, 8:082107–082107–11, 2005.

[18] S. Kumar, P. Vorobieff, G. Orlicz, A. Palekar, C. Tomkins, C. Goodenough, M. Marr-Lyon, K. P. Prestridge, and R. F. Benjamin. Complex flow morphologies in shock-accelerated gaseous flows. *Physica D*, 235:21–28, 2007.

[19] DRS. *DRS's Imacon 200 technical specifications*. DRS Data & Imaging Systems, 138 Bauer Drive, Oakland, NJ 07436.

[20] M. L. Chavez, E. P. Johnson, P. Vorobieff, and C. R. Truman. Experimental studies of shock wave interaction with droplets and particulates. AIAA Paper 2009-4050.